ACS APPLIED MATERIALS & INTERFACES

www.acsami.org

Research Article

Unlocking High-Voltage Cathode Compatibility of Amine-Based Solvents through Enhanced Cation−Solvent Interaction for Rechargeable Mg Batteries

Fei Wang, Yuan Qin, Yuan Tian, Mingteng Zhang, Yu Qiao, Jing Zeng,* and Jinbao Zhao*

Cite This: https://doi.org/10.1021/acsami.5c21669

Read Online

ACCESS | Metrics & More | Article Recommendations | Supporting Information

ABSTRACT: Conventional amine-based electrolytes exhibit superior compatibility with Mg metal anodes, but their practical application is fundamentally constrained by both a restricted electrochemical stability window (<2.0 V on Al foils) and non-negligible high cation desolvation energy barriers. Herein, we first focus on enhancing cation−solvent interaction through a rational high-concentration Li/Mg dual-salt strategy, effectively suppressing free amine solvent molecules and thereby expanding the electrochemical window to exceed 3.0 V. This widened electrochemical window ensures direct compatibility with the industrial Li-ion cathode. Furthermore, to address the high cation desolvation energy barriers and low conductivity in this electrolyte, the ether solvent with a lower coordination ability is introduced into the electrolyte, where part of the ether can participate in the Li^+ solvation structure to alleviate overly strong amine coordination, while the rest can serve as a pseudo-diluent, promoting a reduced cathode desolvation energy barrier and enhanced ion transport. Finally, the Mg//$LiFePO_4$ battery delivers a stable plateau of 2.7 V and a high energy density at the electrode level. This work proposes an efficient electrolyte design paradigm that simultaneously balances Mg anode reversibility, high-voltage cathode compatibility, and a facile preparation method in Mg batteries for the first time, revealing a comprehensive exploration process for high-voltage Mg batteries.

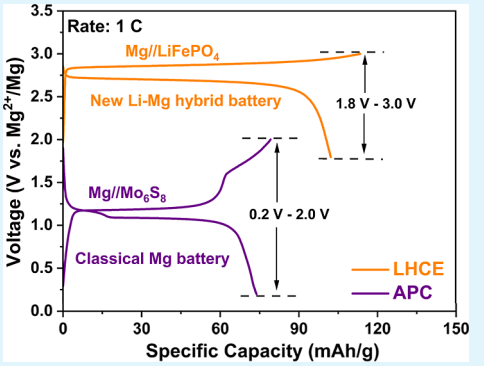

KEYWORDS: *high-voltage stability, high-concentration electrolyte, amine solvent, cation−solvent interaction, Li−Mg hybrid batteries*

1. INTRODUCTION

Rechargeable magnesium (Mg) batteries have attracted considerable interest as a promising post-lithium (Li) era energy storage candidate, driven by their superior theoretical volumetric energy density, cost-effective material availability, and enhanced operational safety.[1−3] However, unlike monovalent Li-based batteries, the strong Coulombic interactions arising from the multivalent ion characteristics impose more severe challenges on the Mg battery system.[4−7] On the cathode side, the high charge density of Mg^{2+} ions induces strong electrostatic interactions with host materials, leading to sluggish ion diffusion kinetics and structural degradation during cycling.[8−10] On the anode side, the formation of passivating surface layers due to the electrolyte decomposition imposes substantial kinetic barriers on Mg plating/stripping processes, leading to the large overpotential and low Coulombic efficiency (CE).[11−14] Therefore, these bottlenecks demand simultaneous breakthroughs in two critical aspects for Mg battery systems: developing an electrolyte system with enhanced anode compatibility and exploring the cathode materials that exhibit operational compatibility with such an electrolyte, which will effectively bridge the gap between the theoretical advantages and practical electrochemical performances.

The electrolyte serves as the ion transport medium within the battery system, simultaneously establishing an interfacial contact between the cathode and the anode. Consequently, the electrolyte directly determines various key performance parameters (such as Mg anode reversibility, ion conductivity, electrochemical window, and cathode compatibility) in the battery system, and the rational design of the electrolyte components including salts and solvents can optimize both the electrochemical performances of electrodes and bulk-phase ion transport behaviors. Due to the severe passivation behavior of the Mg metal anode in conventional electrolytes, this intractable problem requires that early electrolyte engineering focus on designing novel Mg salts with stable anionic structures combined with ether-based solvents (such as Grignard reagents[15−17] and boron-based electrolytes[18,19]) to achieve high reversibility of Mg anodes. While this design

Received: October 29, 2025
Revised: March 3, 2026
Accepted: March 20, 2026

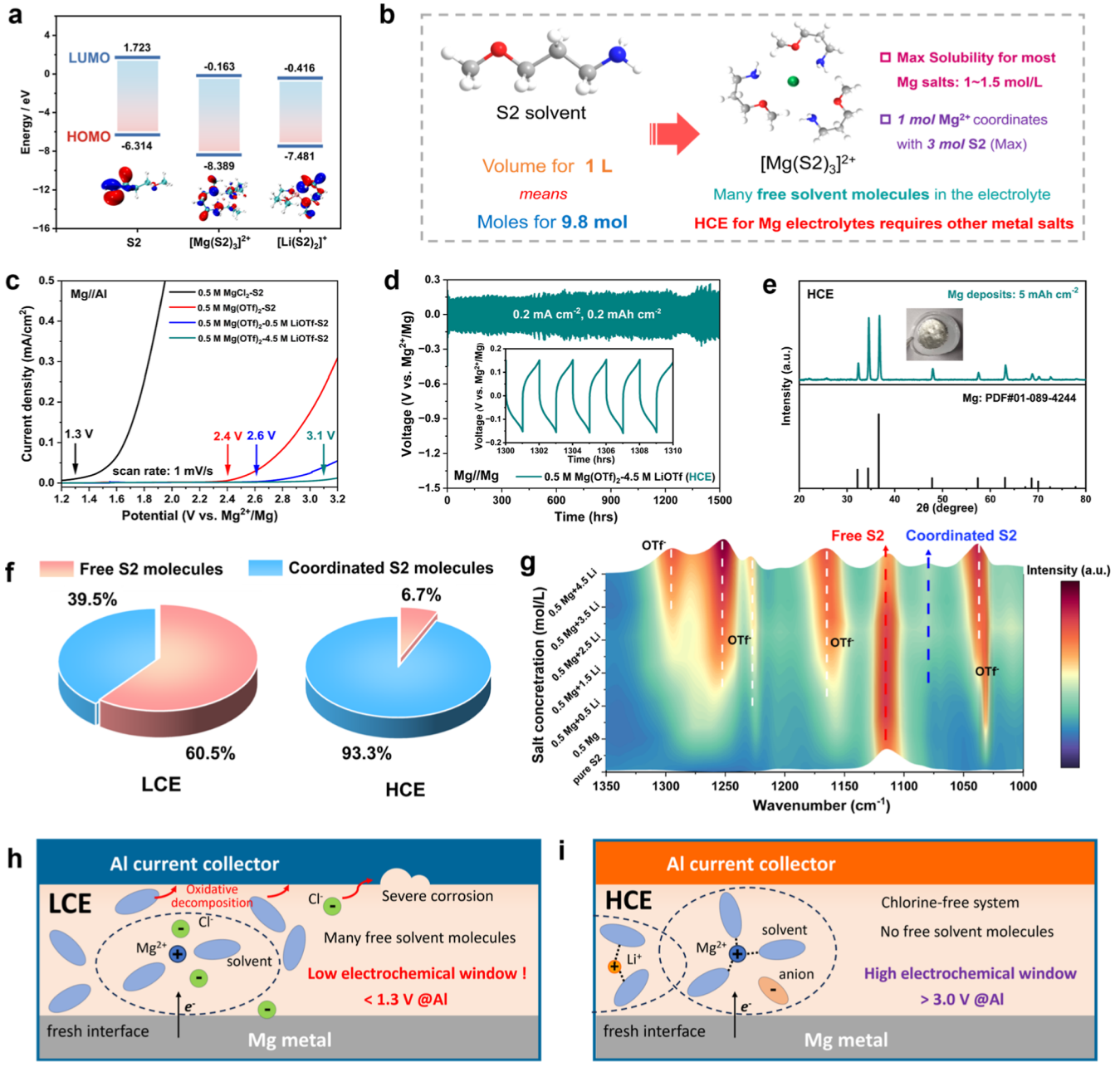

Figure 1. (a) Highest occupied molecular orbital/lowest unoccupied molecular orbital energy levels of the free S2 molecule, $[Mg(S2)_3]^{2+}$ ion cluster, and $[Li(S2)_2]^{+}$ ion cluster. (b) Schematic illustration of the design principle of the HCE with the amine solvent for Mg batteries. (c) The LSV curves of typical amine-based electrolytes. (d) Galvanostatic cycling performance of the optimized HCE electrolyte at 0.2 mA cm^{-2} for 0.2 mAh cm^{-2}. (e) The XRD analysis result of Mg deposits for the optimized HCE at 0.1 mA cm^{-2} for 5.0 mAh cm^{-2} (inset shows the optical picture of Mg deposits for the HCE). (f) The pie charts of the ratios of free S2 molecules and coordinated S2 molecules in LCE and HCE. (g) FTIR spectra of pure S2 and S2 with different salt concentrations. Schematic illustration of the solvation structure and features of (h) the LCE and (i) the HCE.

paradigm effectively addresses anode passivation, it inevitably introduces drawbacks such as high air sensitivity, excessive reagent cost burdens, and complicated preparation procedures. At present, there are virtually no commercially available electrolytes that can simultaneously achieve reversible Mg metal anodes and be compatible with high-voltage cathodes, which severely impede the development of high-energy-density Mg batteries. Notably, recent significant advancements in amine-based electrolyte systems garner considerable attention as these electrolytes demonstrate the feasibility of achieving reversible Mg metal anodes based on conventional electrolyte formulations.[20−24] These emerging amine-based electrolytes exhibit distinct advantages over classic highly reductive electrolyte systems with respect to low cost and commercial availability. Although amine-based electrolytes are widely acknowledged to exhibit favorable compatibility with Mg metal anodes, their limited voltage window (below 2.0 V vs Mg^{2+}/Mg on Al foils) and high cation desolvation energy barriers have emerged as crucial obstacles impeding their further advancement, ultimately restricting the practical energy density to below 100 Wh/kg (when typically coupled with the Mo_6S_8 cathode). Therefore, overcoming the voltage limitations

https://doi.org/10.1021/acsami.5c21669
ACS Appl. Mater. Interfaces XXXX, XXX, XXX−XXX

of amine-based electrolytes and achieving high-voltage cathode compatibility have become critical and pressing challenges in the field of amine-based electrolyte development.[25]

Herein, we propose a high-concentration electrolyte (HCE) and Li/Mg dual-salt design strategies that significantly enhance the cation−solvent interaction through promoting the coordination situation of amine (3-methoxypropylamine, denoted as S2) molecules with cations to reduce the number of free amine solvent molecules, ultimately achieving a greatly expanded electrochemical window exceeding 3.0 V vs Mg^{2+}/Mg on commercial aluminum (Al) current collectors. To address the limited solubility of Mg salts in amine solvents, this hybrid dual-salt system strategically combines a moderate-concentration magnesium triflate ($Mg(OTf)_2$) with a high-concentration lithium triflate (LiOTf). We excluded Cl-based salts due to their inherent corrosivity, with the final selection of OTf^- anions being motivated by their resistance to decomposition in amine solvents. The selection of Li salts can prevent Li^+ co-deposition on the Mg anode interface, while the expanded voltage window of the Li/Mg hybrid electrolyte enables its direct integration with the industrial-grade Li-ion cathode ($LiFePO_4$, LFP) in the full-cell configuration. This paradigm shift effectively bypasses the long-standing challenge in developing suitable Mg cathode materials. Furthermore, we construct a localized high-concentration electrolyte (LHCE) to address the limitation of high cation desolvation energy barriers and low conductivity in this HCE. Since the common diluents in Li electrolytes are not compatible with Mg metal anodes, the ether solvent (dimethoxyethane, DME) with lower coordination ability is selected to establish a special LHCE design model for Mg batteries, in which a small part of DME can participate in the solvation structures, while the rest can serve as the pseudo-diluent. This electrolyte system preserves acceptable Mg anode reversibility and significantly enhances bulk ion transport. Moreover, the partial involvement of DME in Li^+ solvation structures alleviates an overly strong amine coordination situation, thereby reducing the desolvation energy barrier for Li^+ intercalation at the cathode side. Finally, the Mg//LHCE//LFP hybrid system can deliver a high discharge capacity over 100 mAh/g at a rate of 1 C with a stable voltage platform at 2.7 V vs Mg^{2+}/Mg, corresponding to a high energy density of approximately 270 Wh/kg at the electrode level. Traditional Li−Mg dual-salt strategies have focused on utilizing Li salts to improve bulk ion transport and accelerate the intercalation kinetics of low-voltage cathode materials. In contrast, a tailored Li−Mg dual-salt strategy in this work is employed to overcome the inherent solubility limitation of Mg salts in electrolytes, enabling the successful construction of HCEs for Mg batteries. This innovative approach remarkably widened the electrochemical window of pristine amine-based electrolytes. Furthermore, the introduction of ether co-solvent into the HCE effectively improves the bulk transport behavior and reduces the cation intercalation energy barrier at the cathode side. The developed electrolyte system achieves good compatibility with the commercial Li-ion battery cathode material, thereby significantly expanding the range of candidate cathode materials available for Mg batteries. This work establishes a comprehensive exploration process of high-voltage amine-based electrolyte design paradigm through the principle of enhancing cation−solvent interaction.

2. RESULTS AND DISCUSSION

2.1. Analysis of Low Anodic Stability in Amine and the HCE Design

The limited oxidative stability of existing Mg electrolytes containing amine solvents mainly originates from the abundant free amine molecules in the low-concentration electrolyte (LCE) system. The quantum chemical calculation results (Figure 1a) demonstrate that the free amine solvent molecule exhibits a higher-lying highest occupied molecular orbital (HOMO) energy level than their Li^+/Mg^{2+}-coordinated counterparts. Crucially, this coordination triggers the reorganization of electron density in amine molecules, characterized by the directional transfer of nitrogen lone-pair electrons to metal cations, thereby lowering the energy levels of their molecular orbitals. Meanwhile, charge density difference plots for (LiS2-2*S2−Li^+) and (MgS2-3*S2−Mg^{2+}) reveal that the electron density significantly increases around the metal cations (solid lines), indicating charge transfer toward the metal centers upon coordination with free S2 molecules (Figure S1a−d). This electronic reconfiguration enables coordinated amine molecules to resist electron loss at higher operating potentials, intrinsically enhancing their oxidative stability. Besides, oxidative stability is characterized by using the electron-transfer free energy changes from a thermodynamic perspective and overpotentials from a kinetic perspective. As shown is Figure S1e,f, the Laplacian bond order analysis indicates that the S2 molecule is likely to cleave into a $CH_3O^{+\bullet}$cationic radical and a $CH_2CH_2CH_2NH_2^{\bullet}$neutral radical. Subsequently, we employed an implicit solvation model to compute the dissolution Gibbs free energies for both reactants and products. The computed Gibbs free energy for the oxidation of the free S2 molecule (ΔG_{free}) is 240.88 kcal/mol, while that for the coordinated species ($\Delta G_{coordinated}$) is 407.91 kcal/mol. The significantly higher value for $\Delta G_{coordinated}$ indicates a substantial increase in the free energy change for the oxidation reaction upon coordination, demonstrating that coordination enhances the oxidative stability of the S2 molecule, which is consistent with our previous analysis. However, the exact mechanism of the real charge transfer during the coordination process of S2 remains not particularly clear. Consequently, optimizing the coordination state of amine molecules to enhance the cation−solvent interaction through electrolyte concentration engineering emerges as a critical pathway to overcome the oxidative voltage limitations of existing amine-based electrolyte systems (Figure S1g,h).

The engineering of high-concentration amine electrolytes demands not only increasing salt concentration to reduce free solvent molecules but also, more critically, judicious selection of suitable electrolyte salts to meet two essential requirements: the selected anions should exhibit noncorrosive characteristics to prevent side reactions on the cathode current collectors while ensuring reversible Mg plating/stripping behaviors in amine-based electrolytes. Although Cl^- ions can mitigate Mg anode passivation, their intrinsic corrosiveness to most cathode current collectors severely limits the electrochemical window of the electrolyte system. According to our previous work,[23,26,27] OTf^- anions can maintain high interface stability of Mg metal anodes during extended cycling compared to $TFSI^-$ anions. Consequently, $Mg(OTf)_2$ is rationally selected as the optimal Mg salt to implement the HCE for Mg batteries (Figures S2 and S3).[28−31]

https://doi.org/10.1021/acsami.5c21669
ACS Appl. Mater. Interfaces XXXX, XXX, XXX−XXX

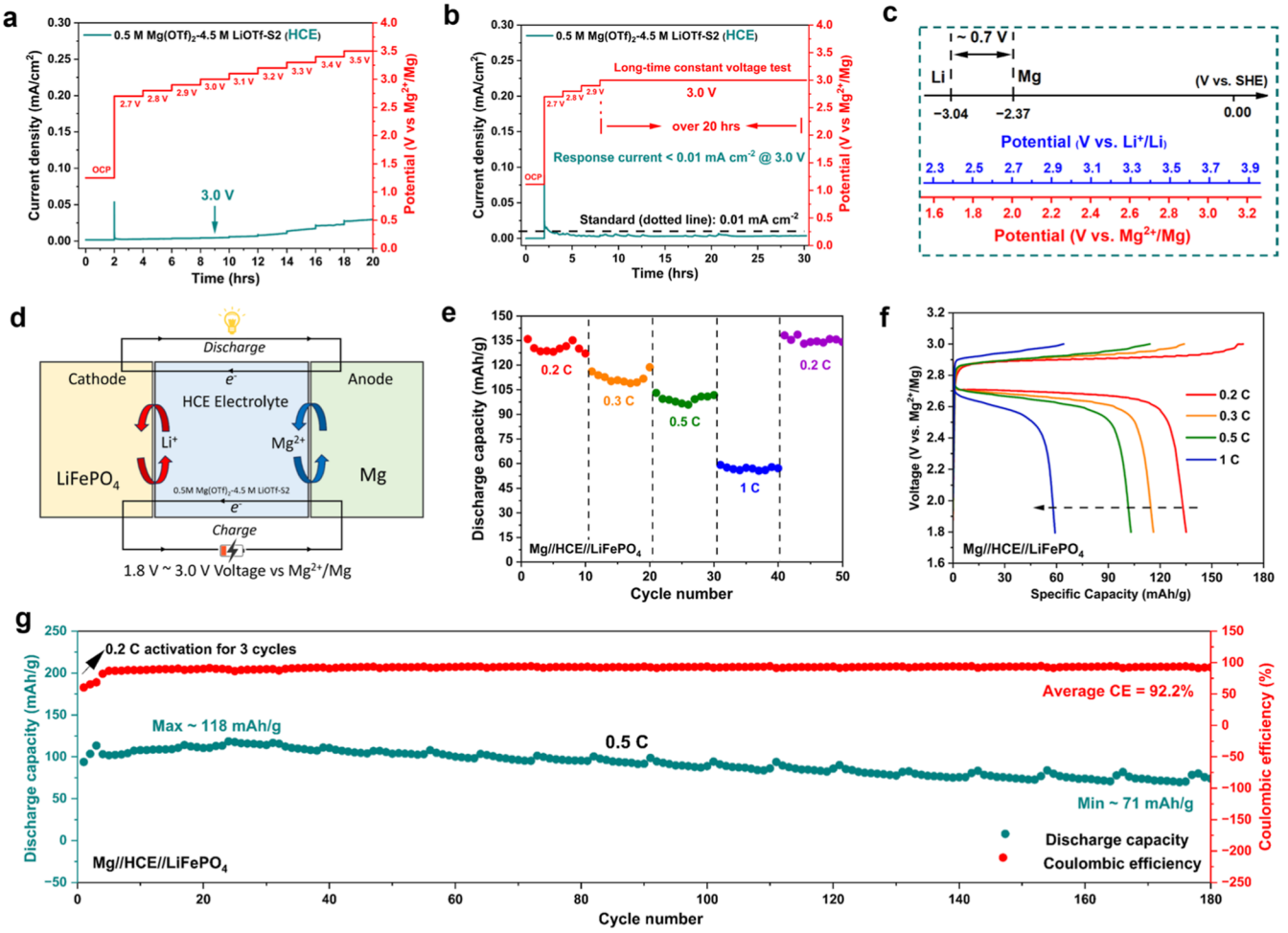

Figure 2. (a) The step potential method test curve of the optimized HCE from open circuit potential (OCP) to 3.5 V. (b) The prolonged constant-voltage test curve of the optimized HCE. (c) Schematic illustration of the voltage difference of the cathode material between Li batteries and Mg batteries. (d) Schematic illustration of the operating principle in the Li/Mg hybrid full cell with the optimized HCE. (e) Rate performance of the optimized HCE in the Mg//LFP full cell from 0.2 to 1 C (0.2 C, 0.3 C, 0.5 C, 1 C, and 0.2 C; 1 C = 150 mA/g). (f) Voltage profiles of the optimized HCE in the Mg//LFP full cell at rates of 0.2 C, 0.3 C, 0.5 C, and 1 C. (g) The long cycling performance of the Mg//LFP full cell with the optimized HCE at a rate of 0.5 C.

The limited solubility of single Mg salts in organic solvents is the primary constraint for the development of HCEs in Mg batteries. As shown in Figure S4, the maximum concentration of $Mg(OTf)_2$ salt in the S2 solvent is defined to be 1.0 mol/L (M) because further increases in the salt concentration result in the electrolyte exhibiting a noticeable color change from colorless and transparent to yellow, accompanied by turbidity and decreased fluidity. Even at this solubility limit, only up to ~30% of amine molecules participate in cation coordination, leaving a substantial number of free amine solvent molecules in the electrolyte system. Consequently, achieving HCEs in Mg batteries through a single Mg salt is fundamentally limited by the inherent solubility limitations of Mg salts, thereby necessitating the incorporation of other co-salts (Figure 1b). Based on our previous experience in electrolyte design,[27] LiOTf is selected as a highly promising salt for formulating HCEs in Mg batteries. The selection of the OTf^- anion identical to that in the Mg salt ensures the reversibility of the Mg metal anode, and more importantly, this high-voltage electrolyte strategy can potentially enable the Li−Mg hybrid system to achieve direct compatibility with commercial Li-ion cathodes.

Because the HCE system requires a Li−Mg hybrid dual-salt approach, optimizing the ratio between Mg and Li salts emerges as a primary consideration in electrolyte engineering. Therefore, we design three HCEs with different Li/Mg salt molar ratios (0.2 M Mg−5.0 M Li, 0.5 M Mg−4.5 M Li, and 1.0 M Mg−3.5 M Li) to investigate their effects on the high-voltage stability and Mg anode performance. As shown in Table S1, the formulations are based on the theoretical assumption that each Mg^{2+} ion coordinates with three S2 molecules and each Li^+ ion coordinates with two S2 molecules, and the coordination demand ($3\times[Mg^{2+}]+2\times[Li^+]$) exceeds the number of S2 solvent molecules in the electrolyte system (9.8 mol). The initial assessment of the electrochemical window for these HCEs is conducted via linear sweep voltammetry (LSV) measurement. LSV measurements in this work all employ Al current collectors because Al foils act as the standard cathode current collectors in commercial Li-ion batteries. As shown in Figures S5 and 1c, these HCEs all exhibit expected high electrochemical stability exceeding 3.0 V on Al foils, indicating the great effectiveness of the HCE strategy for unlocking the anodic stability of amine solvents. Despite exhibiting similar electrochemical windows, these three electrolytes with varying Mg^{2+}/Li^+ molar ratios exhibit

https://doi.org/10.1021/acsami.5c21669
ACS Appl. Mater. Interfaces XXXX, XXX, XXX−XXX

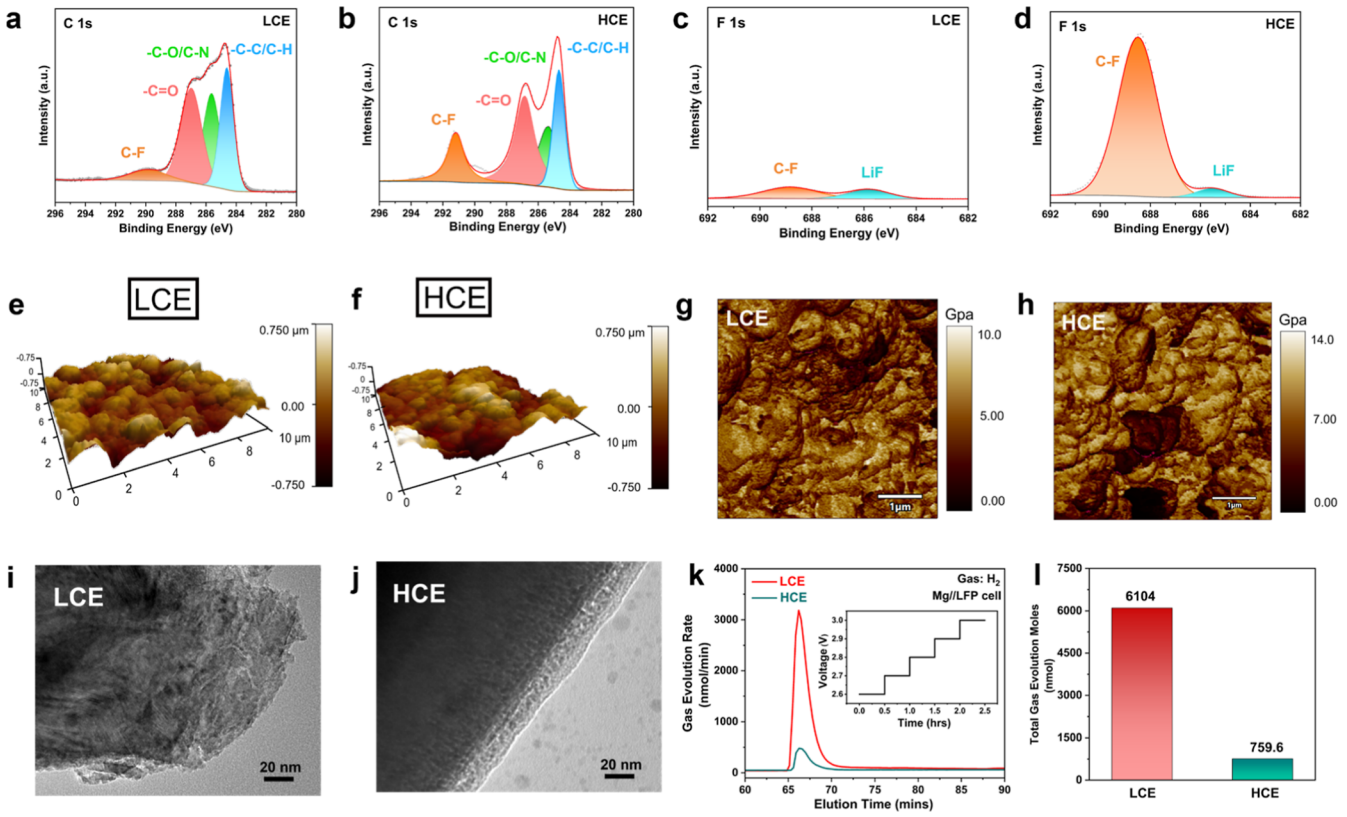

Figure 3. XPS (a) C 1s and (c) F 1s spectra of LFP cathodes of the LCE (Mg//LFP coin cell is cycled at a rate of 0.2 C for the first cycle with the capacity cutoff at 400 mAh/g and detected at the end of the charging state). XPS (b) C 1s and (d) F 1s spectra of LFP cathodes of the HCE (Mg//LFP coin cell is cycled at a rate of 0.2 C for the first cycle and detected at the end of the charging state). (e) Surface morphology and (g) Young's modulus of the LFP cathode operated in the LCE. (f) Surface morphology and (h) Young's modulus of the LFP cathode operated in the HCE. The TEM images of the LFP cathode operated in the (i) LCE and (j) HCE. (k) Gas evolution MS curves of the Mg//LFP with the LCE and the HCE (inset shows the testing process step curve). (l) Comparison of the gas evolution amount in the LCE and HCE.

distinct differences in Mg anode performance (Figure S6a−c). Only the HCE with moderate Mg salt content (0.5 M Mg+4.5 M Li) enables acceptable Mg anode performance at the moderate current density to some extent, and thus, the HCE with this Mg/Li molar ratio is selected as the optimized electrolyte for subsequent testing. Figure S7 displays the optical characterization of this HCE, revealing a pale yellow and transparent appearance with low fluidity. Besides, this HCE can exhibit stable operation with an overpotential of approximately 0.15 V for 1500 h in the Mg//Mg cell (Figure 1d) and exhibits a high average CE of about 99.1% in the Mg//SS cell (Figure S8), demonstrating good compatibility between the HCE and the Mg metal anode. The uniform cycling morphology of the Mg metal surface is confirmed by scanning electron microscopy (SEM) (Figure S9a). To verify whether Mg deposition occurs exclusively without Li co-deposition in this Li/Mg hybrid electrolyte system with an extremely high Li salt concentration (4.5 M), the Mg electrodeposits (0.1 mA cm^{-2} for 5.0 mAh cm^{-2} in a Mg//SS cell) are characterized by X-ray diffraction (XRD) measurement and X-ray photoelectron spectroscopy (XPS) measurement (Figures 1e and S9b). The XRD pattern of the deposited Mg exhibits excellent agreement with the standard Mg phase (PDF#01-089-4244), and no detectable Li peaks are observed by XPS as well. These results confirm the absence of Li co-deposition during electrodeposition.

The ratio of free S2 molecules to total S2 molecules in both the LCE and HCE is investigated by the molecule dynamic simulation (Figure S10a−d and Table S2). The 0.5 M $Mg(OTf)_2$−0.5 M LiOTf−S2 electrolyte is chosen as the representative of the LCE. As shown in Figure 1f, in the LCE, free S2 solvent molecules account for up to 60.5% of the total, indicating that the low salt concentration results in abundant uncoordinated S2 solvent molecules, thus leading to a narrow electrochemical window of the LCE. In sharp contrast, the HCE contains only ∼6.7% free S2 solvent molecules, demonstrating that the significant increase in salt concentration effectively reduces the population of free solvents, consistent with the original design strategy. This is also confirmed by Fourier transform infrared (FTIR) spectroscopy (Figure 1g). With increasing salt concentration, the intensity of the coordinated S2 peak is significantly enhanced, accompanied by a reduction in the free S2 solvent signal, indicating an increased participation of S2 solvent in the coordination structure. In summary, Figure 1h,i schematically illustrates the differences in internal components and solvation structures between the LCE and HCE, respectively. The low cation concentration in the LCE leads to insufficient cation−solvent interactions, resulting in an excessive population of uncoordinated amine molecules that are highly susceptible to oxidative decomposition under a high-voltage operation. Besides, in Cl-containing electrolytes, residual Cl^- anions further exacerbate current collector corrosion on the cathode side and diminish the oxidation stability. In sharp contrast, Cl-free HCE, which is formulated with a moderate concentration of Mg salt and a high concentration of Li salt, features enhanced cation−solvent

https://doi.org/10.1021/acsami.5c21669
ACS Appl. Mater. Interfaces XXXX, XXX, XXX−XXX

coordination. This design enhances cation−solvent interactions, thereby minimizing free solvent molecules and extending the electrochemical stability window to 3.0 V vs Mg^{2+}/Mg on Al current collectors, surpassing that of conventional LCEs.

2.2. Full-Cell Compatibility Assessment through the LFP Cathode

Generally, the LSV measurement cannot accurately determine the electrochemical window of the electrolyte because it strongly depends on scan rates and is prone to hysteresis in the current response. To more precisely determine the electrochemical window of this HCE, the step potential method (Figure 2a) and the prolonged constant voltage test (Figure 2b) are conducted, which further confirms that the electrolyte does not undergo decomposition at specified voltages. The step potential method result indicates that no detectable current response can be observed when the voltage is applied up to 3.0 V vs Mg^{2+}/Mg, and this is further confirmed by the prolonged constant voltage test. The Mg//Al cell employing this HCE maintained at 3.0 V vs Mg^{2+}/Mg for over 20 h consistently exhibits a current response below 0.01 mA cm^{-2}, demonstrating the reliable anodic stability of the HCE at 3.0 V vs Mg^{2+}/Mg. The standard hydrogen electrode (SHE) potential difference between Li metal (−3.04 V vs SHE) and Mg metal (−2.37 V vs SHE) is approximately 0.7 V, indicating that this HCE is compatible with commercial Li-ion battery materials featuring a 3.7 V vs Li^+/Li charge cutoff voltage (Figure 2c). Consequently, lithium iron phosphate is selected as the cathode material for this HCE with a theoretical operating window of 1.8−3.0 V and a 2.8 V discharge plateau (vs Mg^{2+}/Mg). The working mechanism of the hybrid battery is shown in Figure 2d. Since Mg^{2+} ions cannot contribute to the reversible capacity in the LFP cathode (Table S3) and Li co-deposition behavior has been confirmed not to occur as shown above, the cathode side just involves the Li^+ ion intercalation/extraction process, while the anode side only undergoes the Mg metal deposition/stripping process. This design concept simultaneously leverages the intrinsic merits of Mg metal anodes and dramatically broadens the range of cathode selection to include commercial Li-ion counterparts, thereby effectively bypassing the persistent challenge of developing compatible Mg cathode materials through a transformative high-voltage hybrid cell configuration paradigm. For the conventional amine-based LCE, the Mg//LFP full cell cannot operate normally and undergoes electrolyte decomposition when the voltage rises to about 2.7 V vs Mg^{2+}/Mg (Figure S11), which is consistent with the LSV result (Figure 1c). As for the HCE, as shown in Figure 2e,f, the Mg//HCE//LFP full cell can operate at different rates and deliver a discharge capacity of about 105 mAh/g at a rate of 0.5 C (1 C = 150 mA/g). Moreover, this hybrid battery displays a high discharge plateau around 2.7 V vs Mg^{2+}/Mg under various charge/discharge rates, showing general agreement with the previous theoretical prediction. The Mg//HCE//LFP full cell exhibits moderate cycle durability, sustaining 60.1% capacity retention after 180 cycles at a rate of 0.5 C. The CE of full cells which is less than ideal may be attributed to the large cationic desolvation energy barrier caused by amine-based solvents, which calls for further systematic research in the future. The aforementioned tests demonstrate that the HCE strategy successfully fulfills the original design concept of achieving high-voltage stability in amine solvents while exhibiting practical compatibility with commercial Li-ion battery cathode materials.

The characteristics of LFP cathodes after cycling in the LCE and HCE are systematically investigated as well. As shown in Figure 3a−d, XPS reveals a critical distinction in the surface chemistry of the LFP electrodes cycled in the HCE versus those cycled in the LCE. For the HCE system, a substantial accumulation of F-containing species (C−F bonds) is observed on the LFP surface, which is solely attributed to the decomposition of OTf^- anions in the HCE. In contrast, the LCE system exhibits a significantly weakened F content. This disparity is directly linked to the electrochemical stability of the electrolytes during cycling. In the LCE system, the insufficient salt concentration fails to stabilize the electrolyte−electrode interface, leading to premature decomposition of amine solvents, which occurs prior to the onset of Li-ion intercalation/deintercalation. Conversely, in the HCE, free solvent molecules are suppressed through coordination with cations, thus enhancing the oxidative stability of amine solvent and preventing continuous solvent decomposition. Furthermore, the Li^+ solvation structure in the HCE (Figure S10d), enriched with OTf anions, facilitates the formation of an inorganic-rich interface primarily composed of anion-derived decomposition products rather than organic species from solvent degradation. This is further confirmed by atomic force microscopy (AFM) results (Figure 3e−h). The HCE-derived surface displays a higher Young's modulus (average 7.0 GPa) compared to that of the LCE (average 5.0 GPa), which is attributed to the mechanically robust F-rich components (which typically exhibit a higher modulus than organic components). Besides, the F-rich LFP electrode surface in the HCE exhibits a smoother morphology (Ra: 151.6 nm in HCE vs 160.8 nm in LCE). Transmission electron microscopy (TEM) also reveals differences in the surface characteristics of the LFP cathode material cycled in the two electrolytes (Figure 3i,j). In the LCE, nearly no cathode electrolyte interphase (CEI) formation can be observed on the cathode surface due to the LCE-based full cell's inability to complete normal charging. Conversely, a uniform CEI layer is observed on the LFP material cycled in the HCE. The gas generation under high voltage during charging in the battery system is also analyzed by using mass spectrometry (MS) (Figure 3k,l). The testing method involves charging the battery in accordance with designed steps, followed by argon purging to sweep the evolved gases from the system into the MS for analysis. The gas quantity in the LCE (6104 nmol) is obviously higher than that in the HCE (759.6 nmol), indicating that free solvent molecules in the HCE system are significantly suppressed, thereby inhibiting the decomposition of amine groups and gas evolution under the high-voltage condition.

The above full-cell evaluation results combined with the characterizations demonstrate that the Mg//LFP hybrid battery employing this HCE generally meets the initial design expectations. However, the excessively high viscosity and low ionic conductivity of the HCE (Figure S12), combined with the strong coordination of amine molecules (which leads to a significantly higher Li^+ intercalation energy barrier at the cathode side), collectively impede the full realization of the performance potential in full-cell systems. Therefore, it is imperative to further develop a localized high-concentration Li/Mg dual-salt hybrid electrolyte tailored for Mg battery systems derived from this HCE.

https://doi.org/10.1021/acsami.5c21669
ACS Appl. Mater. Interfaces XXXX, XXX, XXX−XXX

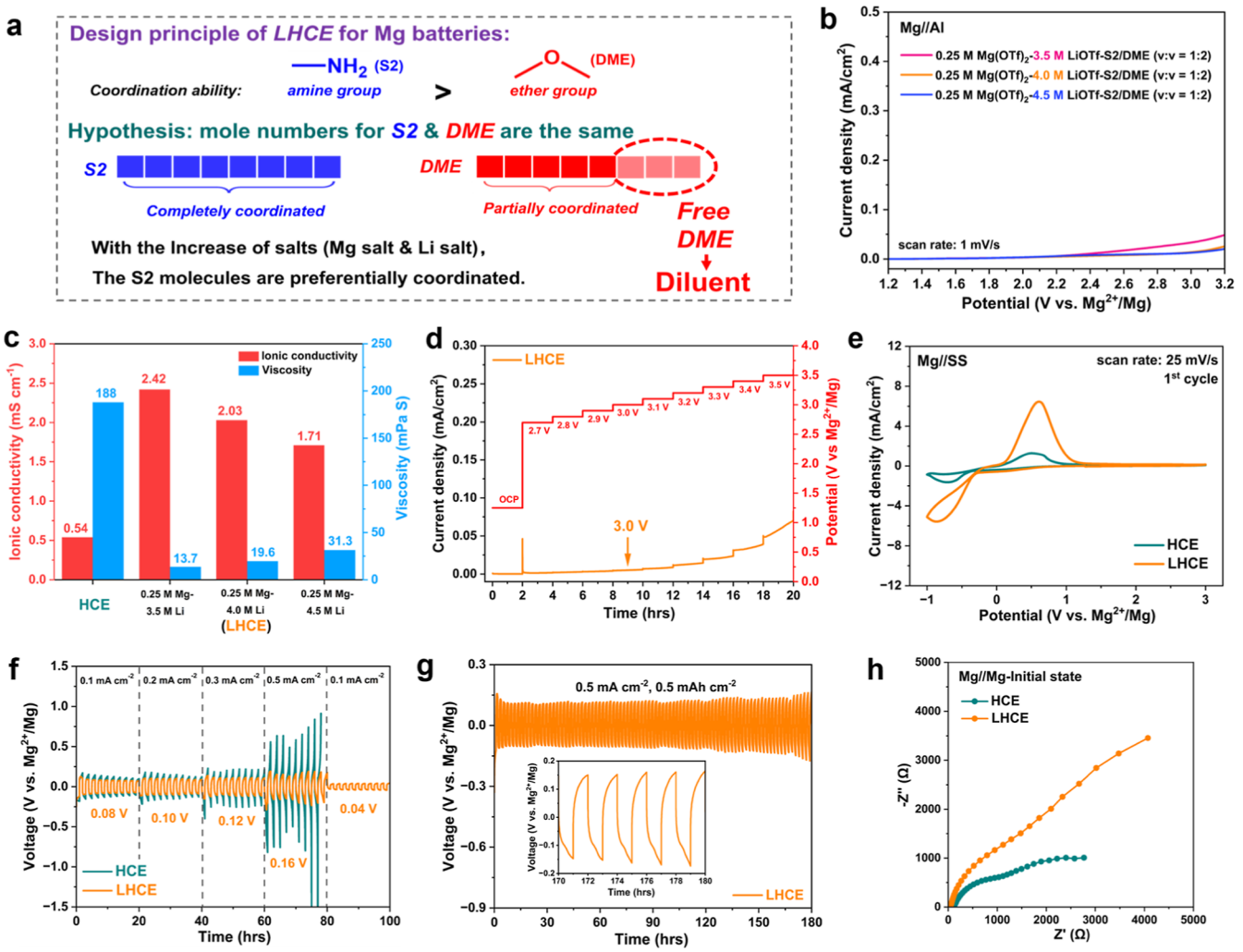

Figure 4. (a) The design principle of the special LHCE for Mg batteries. (b) The LSV curves of three LHCEs with different Li salt concentrations. (c) Ionic conductivities and viscosities of the HCE and three types of LHCEs. (d) The step potential method test curve of the optimized LHCE from OCP to 3.5 V. (e) CV curves of the HCE and the optimized LHCE. (f) The rate performance of the HCE and optimized LHCE at current densities from 0.1 to 0.5 mA cm^{-2} (0.1, 0.2, 0.3, 0.5, and 0.1 mA cm^{-2}) in the Mg//Mg symmetric cells. (g) The long cycling performance of the Mg//Mg symmetric cell with the optimized LHCE at 0.5 mA cm^{-2} for 5.0 mAh cm^{-2}. (h) Nyquist plots of the HCE and optimized LHCE with the Mg metal anode in the initial state.

2.3. Special Pseudo-LHCE Design Model for Mg Batteries

LHCE has emerged as a common strategy in Li metal batteries.[32,33] By introducing an inert diluent (which does not participate in the Li^+ solvation shells but is miscible with the solvent) into the HCE, the LHCE can maintain the original Li^+ solvation structure and therefore can preserve high-voltage stability while reducing viscosity, enhancing ion transport, and reducing salt usage.[34,35] Guided by the experience of LHCE in Li metal batteries, we incorporate 1,1,2,2-tetrafluoroethyl-2,2,3,3-tetrafluoropropyl ether (TTE)[36] and *n*-hexane (HEX)[37] as two alternative diluent candidates into our designed HCE to evaluate their efficacy in achieving the target electrochemical performance. However, the incorporation of these two diluents (TTE and HEX) introduces new challenges to the electrolyte system, including severe Mg metal anode passivation and immiscibility issues with the HCE (Figures S13–S20). These unsuccessful attempts demonstrate that the LHCE for Mg metal batteries cannot simply replicate Li metal battery design principles, necessitating Mg-specific electrolyte design tailored to their unique characteristics.

Considering that conventional ether solvents are recognized to possess higher anodic stability compared with amine solvents, along with good miscibility with each other and the ability to maintain Mg metal anode reversibility in ether–amine blends, we innovatively propose to develop a special LHCE design model for Mg metal batteries through rational utilization of the difference in coordination ability between amine and ether solvents. In general, the coordination ability of amine groups ($-NH_2$) is stronger than that of ether groups (–O–). In this work, we selected S2 and DME solvents as representatives of these two systems, respectively. We hypothesize a binary solvent system with an equimolar S2/DME molar ratio (Figure 4a). Upon adding a small amount of salt (either Li or Mg salts), the stronger coordination ability of amine groups results in more amine molecules participating in coordination compared with ether molecules. With the gradual increase of the salt concentration, amine solvent molecules invariably undergo full coordination first, leaving unbound DME molecules that spontaneously act as the diluent in this system. This hypothesis can be extended to the condition where DME molecules are more abundant than S2 molecules.

https://doi.org/10.1021/acsami.5c21669
ACS Appl. Mater. Interfaces XXXX, XXX, XXX–XXX

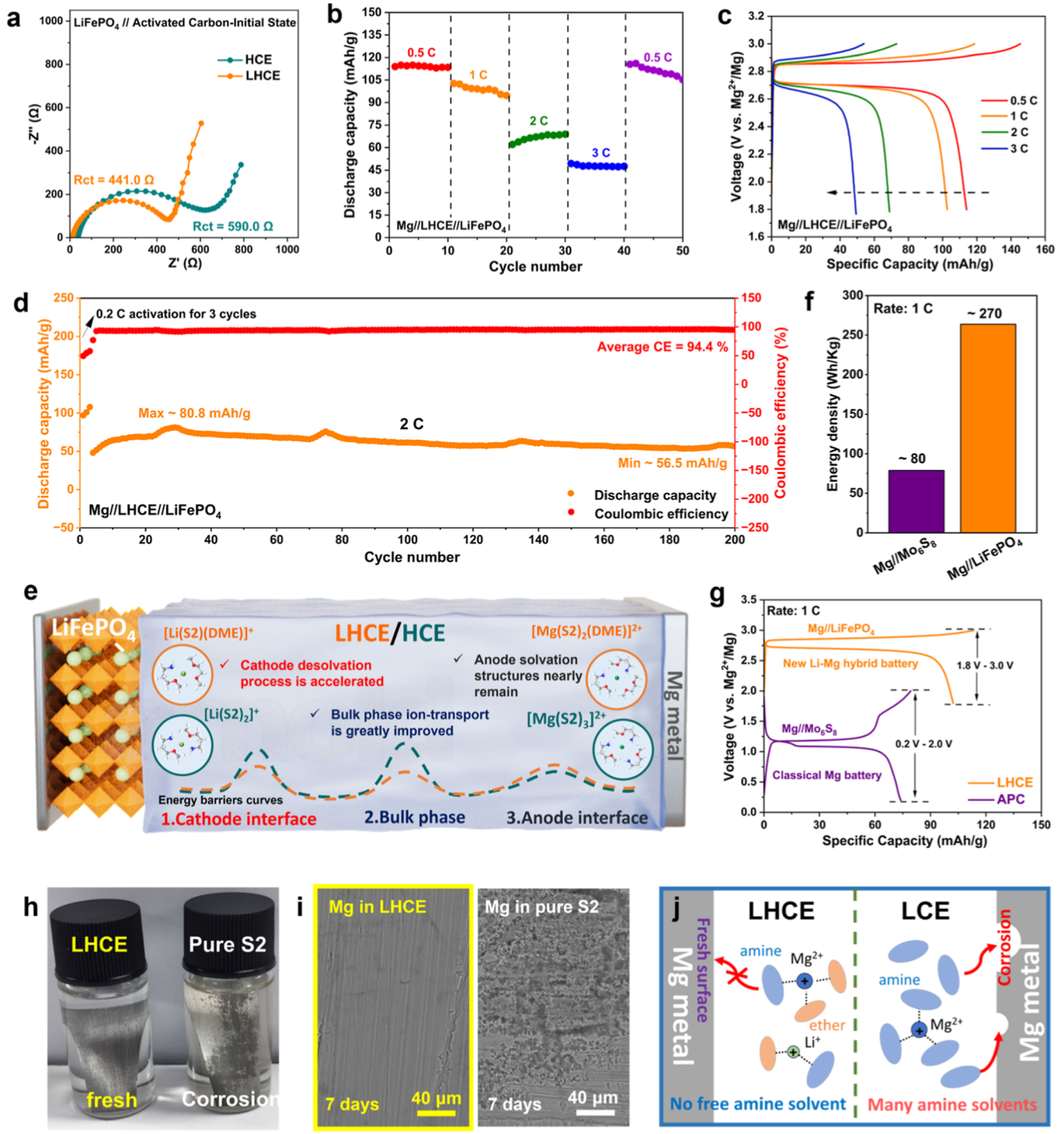

Figure 5. (a) Nyquist plots of the HCE and optimized LHCE with the LFP cathode in the initial state. (b) Rate performance of the optimized LHCE in the Mg//LFP full cell from 0.5 to 3 C (0.5 C, 1 C, 2 C, 3 C, and 0.5 C). (c) Voltage profiles of the optimized LHCE in the Mg//LFP full cell at rates of 0.5 C, 1 C, 2 C, and 3 C. (d) The long cycling performance of the Mg//LFP full cell with the optimized LHCE at a rate of 2 C. (e) Schematic illustration of the full cell optimizing principle of the LHCE compared to the HCE. (f) The histogram of the energy density levels of the Mg//LFP full cell and Mg//Mo_6S_8 full cell at a rate of 1 C (for the Mo_6S_8 cathode, 1 C means 128.8 mA/g). (g) Voltage profiles of the Mg//LFP full cell with the LHCE and the Mg//Mo_6S_8 full cell with the APC electrolyte at a rate of 1 C. (h) The optical image of the Mg foils after immersing in the LHCE and pure S2 solvent for 7 days. (i) The SEM images of the Mg surface morphologies after immersing in the LHCE and pure S2 solvent for 7 days. (j) Schematic illustration of the protection mechanism in the LHCE and the corrosion mechanism in the LCE.

In this design model, the preservation of Mg^{2+} and Li^+ solvation structures is not guaranteed as in the original HCE system. Therefore, DME cannot strictly qualify as a diluent, and the system should be termed a pseudo-localized high-concentration electrolyte (pseudo-LHCE). This is because the introduction of DME alters the solvation structures of the original electrolyte, and thus, it does not act as a traditional non-coordinating diluent as in Li metal batteries. For the sake of simplicity, however, we maintain the original LHCE nomenclature in this work.

https://doi.org/10.1021/acsami.5c21669
ACS Appl. Mater. Interfaces XXXX, XXX, XXX−XXX

The optimized LHCE formulation employs a 1:2 volumetric ratio of S2 to DME solvents. The amount of DME solvent is appropriately increased because, on one hand, more DME molecules result in more diluent molecules in the LHCE, but on the other hand, excessively high DME content will lead to a very low Mg salt concentration, which limits the Mg metal anode performance (because $Mg(OTf)_2$ salt has high solubility only in the S2 solvent). Under these dual constraints of solubility and concentration requirements, the Mg salt concentration is set at 0.25 M to maintain sufficient Mg^{2+} ion availability while avoiding incomplete dissolution. Considering the difficulty in precisely calculating the required Li salt concentration to achieve maximum coordination of the S2 solvent in this system, we design three different Li salt concentrations (3.5, 4.0, and 4.5 M), and subsequently, these three electrolytes are tested through the LSV measurement (Figure 4b). Only the LHCE formulations with 4.0 and 4.5 M LiOTf exhibit expected electrochemical windows. Furthermore, the ionic conductivities and viscosities of these LHCEs and the original HCE are investigated (Figure 4c). Compared with the original HCE, all three LHCE formulations exhibit enhanced conductivities and significantly reduced viscosities, consistent with the design objectives of the LHCE. The comprehensive evaluation incorporating the LSV results and the conductivity−viscosity parameters ultimately identifies the 0.25 M $Mg(OTf)_2$−4.0 M LiOTf−S2/DME (1:2 volumetric ratio) electrolyte as the optimized LHCE. The step potential method (Figure 4d) and the prolonged constant voltage test (Figure S21) results both exhibit no obvious current response at 3.0 V and demonstrate the reliable anodic stability of this LHCE. This is also confirmed by the theoretical calculation and spectral characterization (Figures S22 and S23). The electrochemical test results reveal that the LHCE not only displays a higher response current in the CV measurement (Figures 4e and S24) but also maintains reduced overpotentials at different current densities (especially at 0.5 mA cm^{-2}) in the rate performance test (Figure 4f), demonstrating that the incorporation of diluent successfully modulates physicochemical properties of the electrolyte through viscosity reduction and conductivity enhancement, which facilitate faster ion migration kinetics and improve the rate performance. This is further confirmed by contact angle measurements (Figure S25a−d). Besides, the optical characterization of this LHCE reveals a colorless and transparent appearance with moderate fluidity (Figure S26). The Mg//Mg symmetric cell also shows a stable voltage profile for 180 h with an overpotential of only about 0.15 V at 0.5 mA cm^{-2}, indicating that this LHCE possesses good Mg anode compatibility (Figure 4g). The cycling morphology of the Mg metal surface is investigated by SEM as well (Figure S27). Furthermore, the Mg//SS asymmetric cell (Figure S28) shows an average CE of about 96.0% after 100 cycles, demonstrating that the LHCE can preserve acceptable Mg anode reversibility even after the introduction of a conventional ether-based solvent. The slight decrease in the CE might result from DME-induced elevation of interfacial charge transfer resistance (this promotes the uncontrolled electrolyte decomposition), which is evidenced by the electrochemical impedance spectroscopy (EIS) analysis of the Mg//Mg cell (Figure 4h). The EIS result shows that the LHCE possesses a relatively higher interface charge transfer impedance than that of the HCE. Future efforts should focus on further solvation structure design to restore high anode compatibility for the electrolyte, which is crucial for the ultimate realization of a practical limited-Mg full-cell system. Even a modest difference in CE (such as 96% vs 99%) can translate to a notable distinction in long-term cyclability. Although further optimization of electrolyte components can help alleviate this issue, the current research efforts are primarily dedicated to establishing the LHCE design model for Mg batteries, with applied optimization aspects therefore remaining outside the immediate scope of this study.

Furthermore, variations in cathode interfacial impedance between LHCE and HCE systems are characterized using LFP//activated carbon electrode cell configurations (Figures 5a and S29). Compared to the HCE system, the LHCE system exhibits a significantly lower Rct (441.0 Ω vs 590.0 Ω), indicating that the introduction of DME in the LHCE system can reduce the Li^+ desolvation energy barrier. The DME molecules partially participate in the solvation sheaths and mitigate the overly strong amine-coordination situation in the HCE, which is also confirmed by molecular dynamics simulation (Figure S30a,b). The coordination number of S2 with Li^+ decreases from 1.935 in the HCE to 0.776 in the LHCE, while the coordination number of Li^+−DME is 1.134. These results indicate that the incorporation of DME effectively weakens the strong amine-based coordination of S2 with Li^+. Based on the significant alteration in the Li^+ solvation structure and the remarkable optimization of electrolyte bulk-phase properties, as shown in Figure 5b,c, the Mg//LFP full cell with the LHCE system exhibits an obviously enhanced rate performance compared to the original HCE and can deliver a high discharge capacity of about 105 mAh/g at a rate of 1 C with an average CE of 94.4% (vs about only 60 mAh/g with an average CE of 92.2% for the original HCE). Besides, the Mg//LHCE//LFP full cell can operate stably at a rate of 1 C for 80 cycles, maintaining a discharge capacity of over 100 mAh/g (Figure S31a,b). The long-cycling performance of this system at a higher rate is investigated as well (Figure 5d). The Mg//LHCE//LFP full cell exhibits acceptable cycle stability, sustaining 69.9% capacity retention after 200 cycles at a rate of 2 C, demonstrating the significant potential of the LHCE system for high-rate operation. The XPS and TEM data also reveal the F-rich CEI on the surface of LFP after cycling, which is similar to that observed in the HCE (Figures S32 and S33). In a word, as shown in Figure 5e, compared to the original HCE, the LHCE system strategically sacrifices partial anode performances to significantly enhance bulk ion transport property, and more importantly, the partial participation of DME in Li^+ solvation structures alleviates an overly strong amine-coordination condition in the HCE system, thereby reducing the desolvation barrier for Li^+ insertion at the cathode and ultimately leading to great improvements in full-cell performances. A detailed comparison of the differences between the HCE and the LHCE is shown in Table S4. Compared to the classical Mg//Mo_6S_8 battery with the all-phenyl-complex (APC) electrolyte, this new-type Mg//LFP hybrid battery with the LHCE exhibits a remarkably higher discharge plateau of 2.7 V (vs 1.1 V for the Mg//Mo_6S_8 battery with the APC electrolyte) and a superior discharge capacity exceeding 100 mAh/g (vs 75 mAh/g for the Mg//Mo_6S_8 battery with the APC electrolyte) at a rate of 1 C. This indicates that the Mg//LFP hybrid battery achieves a high energy density of 270 Wh/kg at the electrode level, which is over three times that of the conventional Mg//Mo_6S_8 battery (about only 80 Wh/kg) (Figure 5f,g). Note that the energy density here is estimated by fitting the battery's charge−

https://doi.org/10.1021/acsami.5c21669
ACS Appl. Mater. Interfaces XXXX, XXX, XXX−XXX

discharge curves, rather than calculated based on the actual battery system. However, both its discharge capacity and discharge plateau have been significantly improved compared to traditional Mg batteries. This advancement achieved through the innovative LHCE strategy helps to broaden the cathode compatibility and overcome high-voltage limitations in amine-based Mg batteries. However, the degradation mechanisms of the cathode material in amine-based electrolytes remain unclear and the cycling performance of the full cell is still unsatisfactory, both of which require further targeted investigation. Additionally, excessive free S2 molecules are observed to corrode the Mg metal surface during prolonged immersion (about 7 days), while the LHCE can effectively maintain surface integrity by significantly reducing the number of free S2 molecules (Figure 5h–j). Although amine-based electrolytes demonstrate negligible corrosion of the Mg metal in short-term operation, thereby achieving high CEs in Mg//SS cells, the LHCE system exhibits substantial potential advantages in enhancing the utilization efficiency of Mg metal anodes, particularly critical for future practical Mg-limited battery systems.

3. CONCLUSION

In summary, we propose a high-concentration Li/Mg dual-salt electrolyte design strategy that enhances cation–solvent interaction by promoting coordination between S2 solvent molecules and cations, effectively suppressing free amine molecules and expanding the electrochemical window beyond 3.0 V vs Mg^{2+}/Mg on commercial Al current collectors. The hybrid system combines moderate-concentration $Mg(OTf)_2$ with high-concentration LiOTf to circumvent the low solubility of single Mg salts while avoiding corrosive Cl-based salts. The Li^+ component prevents Li co-deposition at the Mg anode, while the widened voltage window enables direct compatibility with industrial LFP cathodes, bypassing the historical challenge of developing Mg-compatible cathode materials. Furthermore, to mitigate the high viscosity and low conductivity of this HCE, a special LHCE design model for Mg batteries is developed by leveraging the differential coordination abilities of amine and ether solvents. In this design, S2 molecules preferentially coordinate with cations, while excess DME molecules act as the pseudo-diluent. This LHCE preserves acceptable Mg anode reversibility while enhancing bulk ion transport and reducing the Li^+ ion desolvation energy barrier at the cathode side. Finally, the Mg//LHCE//LFP hybrid system achieves a discharge capacity exceeding 100 mAh/g at 1 C with a stable 2.7 V discharge plateau, corresponding to a high energy density of 270 Wh/kg at the electrode level. This work focuses on rational electrolyte design to achieve high anodic stability of amine solvents, with the cathode selection guided by the currently achievable electrochemical window and electrolyte components. The detailed investigations on the cathode material evolution during cycling and intercalation mechanisms are beyond the scope of this work. In the future, the high-voltage electrolyte strategy proposed in this work is expected to facilitate the adoption of higher-voltage Li battery cathode materials in Mg batteries and even extend to sodium-ion (Na-ion) battery cathode materials through the substitution of Li salts with Na salts, alongside more detailed investigations to fully exploit the cost-effectiveness and high-safety advantages of Mg metal anodes in high-voltage hybrid battery systems.

4. EXPERIMENTAL SECTION

4.1. Preparation of Electrolytes

The HCE ($Mg(OTf)_2$–LiOTf-S2) was prepared by simply adding dried $Mg(OTf)_2$ salt and dried LiOTf salt to the dried S2. The salt concentration of the $Mg(OTf)_2$ salt was 0.5 mol/L and the salt concentration of the LiOTf salt was 4.5 mol/L. The electrolyte was magnetically stirred at room temperature until $Mg(OTf)_2$ salt and LiOTf salt were dissolved completely. This dissolution process may take 1 week or even longer because the dissolution rate of $Mg(OTf)_2$ salt in the S2 solvent is very slow (with higher salt concentrations corresponding to longer dissolution durations). The as-prepared electrolyte was further dried overnight with 4 Å molecular sieves three times and then was stored in an argon-filled Braun glovebox for use. The HCEs with other salt concentrations were prepared by the same method, and the concentrations of these electrolytes were according to the molarities mentioned in the text. The LHCEs ($Mg(OTf)_2$–LiOTf-S2/DME) were prepared by the same method of the HCE, and the only difference was that the mixture solvent was prepared by mixing the S2 solvent with DME solvent (volume ratio was 1:2). For the HCEs and LHCEs, all their components including salts as well as solvents and as-prepared electrolytes must be rigorously dried. This step is essential to achieve an ultralow water content in the electrolytes, and only then can the reproducibility of their electrochemical performance be ensured. The LCEs with the $Mg(OTf)_2$ salt and the LiOTf salt of different salt concentrations were prepared by the similar method of the HCE, and the concentrations of these electrolytes were according to the molarities mentioned in the text.

4.2. Material Characterizations

The surface morphology of the samples was examined via SEM (Hitachi S-4800). Crystal structure characteristics were ascertained using XRD (Rigaku Corporation, Japan) equipped with a Cu Kα radiation source at ambient temperature. Infrared spectra were collected with a Fourier infrared spectrometer (FT-IR, Nicolet IS5 spectrometer, Thermo Fisher Scientific Inc.) in attenuated total reflectance (ATR) mode. XPS data were acquired utilizing a PHI Quantum 2000 spectrometer. TEM (Tecnai F30 TWIN, FEI) was employed to assess the morphological features of the LFP material. The mass spectrometry (MS, Hiden, HPR-20 R&D) was utilized for quantifying the gas release rate throughout the battery charging process. The viscosities of the electrolytes were determined at 25 °C by means of a vibratory viscometer (model: SEKONIC VISCOMATE VM-10A series). Electrolyte conductivities were quantified at 25 °C using a high-purity bright platinum electrode with an electrode constant of 1 cm^{-1}. The AC impedance data were collected via a Solartron electrochemical workstation, with an applied voltage amplitude of 10 mV and a frequency window spanning from 10^5 to 1 Hz. The acquired impedance data were subjected to linear fitting, and the experimental conductivities (σexp) were subsequently derived from the following formula:

$$\sigma_{exp} = \frac{1}{R} \cdot \frac{L}{S}$$

where R is extracted from the intercept of the Nyquist plot on the real axis, corresponding to the electrolytic cell resistance. L/S is the electrode constant of the paired platinum electrodes.

4.3. Electrochemical Measurements

CR-2032 coin-type cells were fabricated to assess the cycling stability and rate capability using a Neware standard battery testing system. In these cells, cathode components consisted of Mg foils, stainless steel substrates, Al foils, or $LiFePO_4$ (LFP) material, while Mg foils functioned as anodes and glass fiber membranes were employed as separators. Each coin cell was injected with 200 μL of the electrolyte, and all assembled cells underwent an additional 10 h aging period prior to initiating any electrochemical characterization. Cyclic voltammetry (CV) and linear sweep voltammetry (LSV) measurements were carried out on a CHI 660E electrochemical workstation (Chenhua Co.). For CV tests, the voltage window spanned from −1.0

https://doi.org/10.1021/acsami.5c21669
ACS Appl. Mater. Interfaces XXXX, XXX, XXX–XXX

to 3.0 V, with the initial potential set to the open-circuit value and the scan initiating in the negative direction. Electrochemical impedance spectroscopy (EIS) data were collected over a frequency range from 10^5 Hz to 10^{-1} Hz. Symmetrical cell tests were performed with identical 1.0 h charging and discharging durations. Asymmetrical cell evaluations adopted a 1.0 h discharge time and a charge cutoff voltage of 1.0 V relative to the Mg^{2+}/Mg redox couple. Full-cell performance was tested at various rates (where 1 C was defined as 150 mAh/g) within a charge−discharge voltage interval of 1.8−3.0 V. The mass loading of the LFP cathode material was approximately 1.5 mg/cm^2, and all charge−discharge processes were conducted under constant-current conditions. All electrochemical measurements were implemented at a controlled temperature of 25 °C.

■ ASSOCIATED CONTENT

Supporting Information

The Supporting Information is available free of charge at https://pubs.acs.org/doi/10.1021/acsami.5c21669.

Addition experimental details; calculation methods; supplementary electrochemical performances and spectroscopic characterization results; photos of electrolytes; morphologies of electrodeposits; simulation calculation data; and comparison of the results in LCE, HCE, and LHCE designs (PDF)

■ AUTHOR INFORMATION

Corresponding Authors

Jing Zeng − *College of Chemistry and Chemical Engineering, State-Province Joint Engineering Laboratory of Power Source Technology for New Energy Vehicle, State Key Laboratory of Physical Chemistry of Solid Surfaces, Engineering Research Center of Electrochemical Technology, Ministry of Education, Collaborative Innovation Center of Chemistry for Energy Materials, Xiamen University, Xiamen 361005, P. R. China*; Email: zengjing@xmu.edu.cn

Jinbao Zhao − *College of Chemistry and Chemical Engineering, State-Province Joint Engineering Laboratory of Power Source Technology for New Energy Vehicle, State Key Laboratory of Physical Chemistry of Solid Surfaces, Engineering Research Center of Electrochemical Technology, Ministry of Education, Collaborative Innovation Center of Chemistry for Energy Materials, Xiamen University, Xiamen 361005, P. R. China*; orcid.org/0000-0002-2753-7508; Email: jbzhao@xmu.edu.cn

Authors

Fei Wang − *College of Chemistry and Chemical Engineering, State-Province Joint Engineering Laboratory of Power Source Technology for New Energy Vehicle, State Key Laboratory of Physical Chemistry of Solid Surfaces, Engineering Research Center of Electrochemical Technology, Ministry of Education, Collaborative Innovation Center of Chemistry for Energy Materials, Xiamen University, Xiamen 361005, P. R. China*

Yuan Qin − *College of Chemistry and Chemical Engineering, State-Province Joint Engineering Laboratory of Power Source Technology for New Energy Vehicle, State Key Laboratory of Physical Chemistry of Solid Surfaces, Engineering Research Center of Electrochemical Technology, Ministry of Education, Collaborative Innovation Center of Chemistry for Energy Materials, Xiamen University, Xiamen 361005, P. R. China*

Yuan Tian − *College of Chemistry and Chemical Engineering, State-Province Joint Engineering Laboratory of Power Source Technology for New Energy Vehicle, State Key Laboratory of Physical Chemistry of Solid Surfaces, Engineering Research Center of Electrochemical Technology, Ministry of Education, Collaborative Innovation Center of Chemistry for Energy Materials, Xiamen University, Xiamen 361005, P. R. China*

Mingteng Zhang − *College of Chemistry and Chemical Engineering, State-Province Joint Engineering Laboratory of Power Source Technology for New Energy Vehicle, State Key Laboratory of Physical Chemistry of Solid Surfaces, Engineering Research Center of Electrochemical Technology, Ministry of Education, Collaborative Innovation Center of Chemistry for Energy Materials, Xiamen University, Xiamen 361005, P. R. China*

Yu Qiao − *College of Chemistry and Chemical Engineering, State-Province Joint Engineering Laboratory of Power Source Technology for New Energy Vehicle, State Key Laboratory of Physical Chemistry of Solid Surfaces, Engineering Research Center of Electrochemical Technology, Ministry of Education, Collaborative Innovation Center of Chemistry for Energy Materials, Xiamen University, Xiamen 361005, P. R. China*; orcid.org/0000-0002-2191-3875

Complete contact information is available at: https://pubs.acs.org/10.1021/acsami.5c21669

Notes

The authors declare no competing financial interest.

■ ACKNOWLEDGMENTS

The authors gratefully acknowledge the Natural Science Foundation of Xiamen, China (No. 3502Z202471026), Natural Science Foundation of China (Nos. 22005257 and 22021001), and Natural Science Foundation of Fujian Province of China (No. 2020J05009) for financial support.

■ REFERENCES

(1) Zhang, J.; Chang, Z.; Zhang, Z.; Du, A.; Dong, S.; Li, Z.; Li, G.; Cui, G. Current Design Strategies for Rechargeable Magnesium-Based Batteries. *ACS Nano* **2021**, *15* (10), 15594−15624.

(2) Bonnick, P.; Muldoon, J. A. Trip to Oz and a Peak Behind the Curtain of Magnesium Batteries. *Adv. Funct. Mater.* **2020**, *30* (21), 1910510.

(3) Liang, Z.; Ban, C. Strategies to Enable Reversible Magnesium Electrochemistry: From Electrolytes to Artificial Solid-Electrolyte Interphases. *Angew. Chem., Int. Ed.* **2021**, *60* (20), 11036−11047.

(4) Muldoon, J.; Bucur, C. B.; Gregory, T. Quest for Nonaqueous Multivalent Secondary Batteries: Magnesium and Beyond. *Chem. Rev.* **2014**, *114* (23), 11683−11720.

(5) Yoo, H. D.; Shterenberg, I.; Gofer, Y.; Gershinsky, G.; Pour, N.; Aurbach, D. Mg rechargeable batteries: an on-going challenge. *Energy Environ. Sci.* **2013**, *6* (8), 2265−2279.

(6) Ma, Z.; MacFarlane, D. R.; Ka, M. Mg Cathode Materials and Electrolytes for Rechargeable Mg Batteries: A Review. *Batteries Supercaps* **2019**, *2* (2), 115−127.

(7) Mohtadi, R.; Tutusaus, O.; Arthur, T. S.; Zhao-Karger, Z.; Fichtner, M. The metamorphosis of rechargeable magnesium batteries. *Joule* **2021**, *5* (3), 581−617.

(8) Chen, S.; Fan, S.; Li, H. A.; Shi, Y. M.; Yang, H. Y. Recent advances in kinetic optimizations of cathode materials for rechargeable magnesium batteries. *Coord. Chem. Rev.* **2022**, *466*, 214597.

(9) Qin, K. Q.; Huang, J. H.; Holguin, K.; Luo, C. Recent advances in developing organic electrode materials for multivalent rechargeable batteries. *Energy Environ. Sci.* **2020**, *13* (11), 3950−3992.

(10) Mao, M. L.; Gao, T.; Hou, S. Y.; Wang, C. S. A critical review of cathodes for rechargeable Mg batteries. *Chem. Soc. Rev.* **2018**, *47* (23), 8804−8841.

(11) Li, Y. Q.; Guan, S. L.; Huo, H.; Ma, Y. L.; Gao, Y. Z.; Zuo, P. J.; Yin, G. P. A Review of Magnesium Aluminum Chloride Complex Electrolytes for Mg Batteries. *Adv. Funct. Mater.* **2021**, *31*, 22.
(12) Shuai, H.; Xu, J.; Huang, K. Progress in retrospect of electrolytes for secondary magnesium batteries. *Coord. Chem. Rev.* **2020**, *422*, 213478.
(13) Deivanayagam, R.; Ingram, B. J.; Shahbazian-Yassar, R. Progress in development of electrolytes for magnesium batteries. *Energy Storage Mater.* **2019**, *21*, 136−153.
(14) Zhang, Z. H.; Cui, Z. L.; Qiao, L. X.; Guan, J.; Xu, H. M.; Wang, X. G.; Hu, P.; Du, H. P.; Li, S. Z.; Zhou, X. H.; et al. Novel Design Concepts of Efficient Mg-Ion Electrolytes toward High-Performance Magnesium-Selenium and Magnesium-Sulfur Batteries. *Adv. Energy Mater.* **2017**, *7* (11), 10.
(15) Aurbach, D.; Lu, Z.; Schechter, A.; Gofer, Y.; Gizbar, H.; Turgeman, R.; Cohen, Y.; Moshkovich, M.; Levi, E. Prototype systems for rechargeable magnesium batteries. *Nature* **2000**, *407* (6805), 724−727.
(16) Aurbach, D.; Schechter, A.; Moshkovich, M.; Cohen, Y. On the mechanisms of reversible magnesium deposition processes. *J. Electrochem. Soc.* **2001**, *148* (9), A1004−A1014.
(17) Mizrahi, O.; Amir, N.; Pollak, E.; Chusid, O.; Marks, V.; Gottlieb, H.; Larush, L.; Zinigrad, E.; Aurbach, D. Electrolyte solutions with a wide electrochemical window for recharge magnesium batteries. *J. Electrochem. Soc.* **2008**, *155* (2), A103−A109.
(18) Carter, T. J.; Mohtadi, R.; Arthur, T. S.; Mizuno, F.; Zhang, R.; Shirai, S.; Kampf, J. W. Boron clusters as highly stable magnesium-battery electrolytes. *Angew. Chem., Int. Ed.* **2014**, *53* (12), 3173−3177.
(19) Du, A. B.; Zhang, Z. H.; Qu, H. T.; Cui, Z. L.; Qiao, L. X.; Wang, L. L.; Chai, J. C.; Lu, T.; Dong, S. M.; Dong, T. T.; et al. An efficient organic magnesium borate-based electrolyte with non-nucleophilic characteristics for magnesium-sulfur battery. *Energy Environ. Sci.* **2017**, *10* (12), 2616−2625.
(20) Hou, S.; Ji, X.; Gaskell, K.; Wang, P.-F.; Wang, L.; Xu, J.; Sun, R.; Borodin, O.; Wang, C. Solvation sheath reorganization enables divalent metal batteries with fast interfacial charge transfer kinetics. *Science* **2021**, *374* (6564), 172−178.
(21) Zhang, D.; Wang, Y. R.; Yang, Y.; Zhang, Y.; Zhao, Y. Z.; Pan, M.; Sun, Y. K.; Chen, S. P.; Liu, X. S.; Wang, J. L.; et al. Constructing Efficient Mg(CF3SO3)2 Electrolyte via Tailoring Solvation and Interface Chemistry for High-Performance Rechargeable Magnesium Batteries. *Adv. Energy Mater.* **2023**, *13*, 2301795.
(22) Du, Y. Y.; Chen, Y. M.; Tan, S. S.; Chen, J. L.; Huang, X. T.; Cui, L. M.; Long, J. C.; Wang, Z. T.; Yao, X. H.; Shang, B.; et al. Strong solvent coordination effect inducing gradient solid-electrolyte-interphase formation for highly efficient Mg plating/stripping. *Energy Storage Mater.* **2023**, *62*, 102939.
(23) Wang, F.; Hua, H. M.; Wu, D. Z.; Li, J. L.; Xu, Y. Q.; Nie, X. Z.; Zhuang, Y. C.; Zeng, J.; Zhao, J. B. Solvent Molecule Design Enables Excellent Charge Transfer Kinetics for a Magnesium Metal Anode. *ACS Energy Lett.* **2023**, *8*, 780−789.
(24) Li, Z.; Nguyen, D. T.; Bazak, J. D.; Han, K. S.; Chen, Y.; Prabhakaran, V.; Le, T. T.; Cheng, Z. Z.; Song, M. Y.; Pol, V. G.; et al. Stable Cycling of Mg Metal Anodes by Regulating the Reactivity of Mg2+ Solvation Species. *Adv. Energy Mater.* **2024**, *14* (16), 2301544.
(25) Yang, L.; Du, A. B.; Lv, Z. L.; Zhang, Z. H.; Li, G. C. Emerging amine-assisted electrolytes for rechargeable magnesium metal batteries: Current understanding and future direction. *Chem. Eng. J.* **2025**, *506*, 160376.
(26) Hua, H. M.; Wang, F.; Wang, F.; Wu, J. Y.; Xu, Y. Q.; Zhuang, Y. C.; Zeng, J.; Zhao, J. B. Machine learning molecular dynamics insight into high interface stability and fast kinetics of low-cost magnesium chloride amine electrolyte for rechargeable magnesium batteries. *Energy Storage Mater.* **2024**, *70*, 103470.
(27) Wang, F.; Hua, H. M.; Zhuang, Y. C.; Wu, J. Y.; Zeng, J.; Zhao, J. B. A Li/Mg Double-Salt Strategy Based on Amine Solvent Achieves Bulk Phase-Interface-Electrode Multi-Scale Optimization for Mg Metal Batteries. *Adv. Funct. Mater.* **2025**, *35*, 2414181.
(28) Chinnadurai, D.; Li, Y. J.; Zhang, C.; Yang, G. L.; Lieu, W. Y.; Kumar, S.; Xing, Z. X.; Liu, W.; Seh, Z. W. Chloride-Free Electrolyte Based on Tetrabutylammonium Triflate Additive for Extended Anodic Stability in Magnesium Batteries. *Nano Lett.* **2023**, *23* (23), 11233−11242.
(29) Huang, X. T.; Tan, S. S.; Chen, J. L.; Que, Z. W.; Deng, R. R.; Long, J. C.; Xiong, F. Y.; Huang, G. S.; Zhou, X. Y.; Li, L. J.; et al. Asymmetric SO3CF3–Grafted Boron-Center Anion Enables Boron-Containing Interphase for High-Performance Rechargeable Mg Batteries. *Adv. Funct. Mater.* **2024**, *34* (17), 11.
(30) Dharmaraj, V. R.; Sarkar, A.; Huang, J. Y.; Huang, S. C.; Kuo, C. L.; Wu, C. C.; Chang, W. S.; Chen, H. C.; Lin, Y. P.; Kaun, C. C.; et al. Superionic Quasi-Solid-State Electrolyte for Rechargeable Magnesium-Oxygen Batteries. *ACS Mater. Lett.* **2025**, *7* (4), 1440−1446.
(31) Xiao, J. H.; Wang, H. G.; Yang, A. Q.; Zeng, Q.; Xu, J. M.; Gao, X.; Zhou, J. C.; Tong, J. M.; Liao, C.; Yan, H.; et al. Dual-Functional Electrolyte Additives to Enhance Magnesium Plating/Stripping Performance for Rechargeable Magnesium Metal Batteries With Pure Amine Solvents. *Adv. Funct. Mater.* **2025**, *36*, No. e19527.
(32) Cao, X.; Gao, P. Y.; Ren, X. D.; Zou, L. F.; Engelhard, M. H.; Matthews, B. E.; Hu, J. T.; Niu, C. J.; Liu, D. Y.; Arey, B. W.; et al. Effects of fluorinated solvents on electrolyte solvation structures and electrode/electrolyte interphases for lithium metal batteries. *Proc. Natl. Acad. Sci. U.S.A.* **2021**, *118* (9), 9.
(33) He, R.; Deng, K. R.; Mo, D. Z.; Guan, X. C.; Hu, Y. Y.; Yang, K.; Yan, Z. H.; Xie, H. J. Active Diluent-Anion Synergy Strategy Regulating Nonflammable Electrolytes for High-Efficiency Li Metal Batteries. *Angew. Chem., Int. Ed.* **2024**, *63* (7), 11.
(34) Chen, J.; Zhang, H.; Fang, M. M.; Ke, C. M.; Liu, S.; Wang, J. H. Design of Localized High-Concentration Electrolytes via Donor Number. *ACS Energy Lett.* **2023**, *8* (4), 1723−1734.
(35) Bergstrom, H. K.; McCloskey, B. D. Ion Transport in (Localized) High Concentration Electrolytes for Li-Based Batteries. *ACS Energy Lett.* **2024**, *9* (2), 373−380.
(36) Li, M. H.; Liu, Y.; Yang, X. M.; Zhang, Q.; Cheng, Y. F.; Deng, L.; Zhou, Q. W.; Cheng, T.; Gu, M. D. Acetonitrile-Based Local High-Concentration Electrolytes for Advanced Lithium Metal Batteries. *Adv. Mater.* **2024**, *36* (36), 11.
(37) Kim, M.; An, J.; Shin, S. J.; Hwang, I.; Lee, J.; Park, Y.; Kim, J.; Park, E.; Kim, J.; Park, G.; et al. Anti-corrosive electrolyte design for extending the calendar life of lithium metal batteries. *Energy Environ. Sci.* **2024**, *17* (16), 6079−6090.

https://doi.org/10.1021/acsami.5c21669
ACS Appl. Mater. Interfaces XXXX, XXX, XXX−XXX